Bull. Mater. Sci. (2019) 42:188
https://doi.org/10.1007/s12034-019-1889-y

Electrochemical, thermodynamic and theoretical study on anticorrosion performance of a novel organic corrosion inhibitor in 3.5% NaCl solution for carbon steel

A R HOSEINZADEH and S JAVADPOUR*
Department of Materials Science and Engineering, School of Engineering, Shiraz University, Shiraz, Iran
*Author for correspondence (javadpor@shirazu.ac.ir)

MS received 16 November 2018; accepted 12 March 2019; published online 4 June 2019

Abstract. The theoretical and electrochemical performance of a novel organic corrosion inhibitor 3,4′-dihydro-3-[2′-mercaptothiazolidine]indol-2-one (DMI), for API 5L Grade B carbon steel in 3.5% NaCl, was evaluated by potentiodynamic polarization (Tafel), electrochemical impedance spectroscopy (EIS) and density functional theory (DFT) for quantum chemical studies. Potentiodynamic studies confirmed that DMI was a mixed organic corrosion inhibitor type which specially affects the cathodic branch. The inhibition efficiencies of reactants, DMI and acetylcysteine followed the following order at 25°C and 200 ppm: DMI (87%) > isatin (71%) > 2-thiazoline-2-thiol (62%) > acetylcysteine (54%). EIS measurements illustrated the charge transfer controlled corrosion process. The Langmuir adsorption isotherm model of DMI was adopted. Surface studies were performed using scanning electron microscopy. Activation and adsorption thermodynamic parameters of DMI were computed. The magnitude of ΔG°_{ads} and the sign of ΔH°_{ads} concluded that the adsorption occurred through chemisorption. Quantum chemical calculations of four corrosion inhibitors were used for investigating the molecular structure effect on inhibition efficiency.

Keywords. API 5L Grade B carbon steel; organic corrosion inhibitor; electrochemical techniques; DFT.

1. Introduction

Carbon steel is an economical and ordinary material under alkaline, acidic and salty environments. Salty solutions are used in industrial environments such as cooling water due to both economic and ecological aspects. The corrosion in salt solutions can be very aggressive in many cases [1]. A 3.5% sodium chloride (NaCl) solution was utilized usually in order to perform corrosion for laboratory testing purpose and was recognized to be more corrosive than seawater [2].

The five ways of protecting materials from corrosion include the selection of material, design change, cathodic protection, coatings and corrosion inhibitors. Corrosion inhibitors were usually applied to decrease the degradation of metals. These molecules were adsorbed on the surface of metals and diminished the corrosion process. It is well known that organic compounds inhibit corrosion.

Organic corrosion inhibitors are generally used in industrial systems because of their effectiveness under a wide range of conditions, good solubility in water and oil, low cost and low toxicity. These compounds act as cathodic, anodic or mix inhibitors. Cathodic inhibitors move the corrosion potential toward lower values and inhibit or delay the cathodic reactions (hydrogen evolution and oxygen reduction). In contrast, anodic inhibitors move the corrosion potential in the direction of positive values, react with the metal cation to form an insoluble hydroxide and block the active sites on the metal surface, which prevents anodic reactions (dissolution of the metal) thus reducing the corrosion rate. Mixed inhibitors affect both cathodic and anodic reactions and provide the highest corrosion protection. The action mechanism of organic corrosion inhibitors is based on the adsorption on the surface to form a protective film which displaces water from the metal surface and protect it against corrosion [3].

$$\mathrm{Org} + \mathrm{H_2O_{ads}} \rightarrow \mathrm{Org_{ads}} + \mathrm{H_2O} \quad (1)$$

Adsorption mechanisms of organic inhibitors could be described by chemisorption interaction ability or physisorption [4]. Physisorption is related to electrostatic interactions while chemisorption involves charge transfer from the inhibitors to the surface of the metal. In the former, the adsorption heat is low and the adsorbed species can be detached from the metal surface with increasing temperature, but in the latter, the enthalpy of adsorption is high and electrons transfer from the corrosion inhibitor to the unoccupied d-orbit of transition metals and the bonds are stronger than physisorption with increasing temperature. Inhibitor adsorption is related to inhibitor molecule characteristics, such as electron density, electronic structure and orbital character of the molecule. In organic molecules, the inhibition efficiency of heteroatoms was as follows: O < N < S < P, which will cause to decrease the corrosion degradation on carbon steel [5]. The main parameters which influence the inhibition efficiency are

Table 1. Literature review of organic corrosion inhibitors on the carbon steel surface.

Organic corrosion inhibitor	Environment	Inhibitor efficiency (%)	References
40 ppm *N*,*N*-bis(phosphonomethyl)glycine + 30 ppm Zn^{2+}	200 ppm NaCl	85.2	[11]
20 ppm *N*,*N*-bis(phosphonomethyl)glycine + 30 ppm Zn^{2+} + 100 ppm citrate	200 ppm NaCl	92.8	
1 mM $NaNO_2$ + 1 mM Na_2MoO_4	10 mM NaCl	88	
Sodium butanoate	10 mM NaCl	95	
Sodium hexanoate		98	
Sodium dodecanoate		27	
Sodium stearate		11	
6 mM hexanoate	0.01 M NaCl	92	
3 mM sebacate	10 mM NaCl	94	
100 ppm sodium tripolyphosphate	3% NaCl	85.4	[12]
20 fatty amides with 500 ppm sodium sulphite	3.5% NaCl	80	[13]
0.001 M 1-butyl-3-methylimidazolium chloride	3.5% NaCl	66.6	[14]
100 ppm pyrrole	3.5% NaCl	30.7	[15]
0.2 g l^{-1} zinc gluconate	0.5% NaCl	72.9	[16]
25 ppm hydroxyethyl (HEI-12)	3% NaCl	21	[17]
10^{-3} M of guanine	200 ppm NaCl	91	[18]
10^{-3} M of adenine		82	
10^{-3} M of cytosine		71	
10^{-3} M of thymine		60	
10^{-3} M of glycine		38	
80 mM sodium caprylate	3.5% NaCl	74	[19]

temperature, testing environment and the functional groups of inhibitor molecules [6].

Organic corrosion inhibitors can be divided into some chemical structures with specific elements; some of these compounds containing nitrogen are: amines, pyridine derivatives, triazole derivatives, Schiff base, amino acids and indazole [7,8], nitrogen and sulphur: imidazole derivatives, thiadiazole derivatives and thiazole derivatives [9], nitrogen and oxygen: oxazole derivatives, phthalimides and plant extracts [10]. Table 1 shows the literature review of the anti-corrosion performance of organic inhibitors on the carbon steel surface in NaCl solutions.

The purpose of this research was to investigate the inhibiting effect of a new organic corrosion inhibitor with chemical functional groups containing nitrogen, sulphur and oxygen on the corrosion of carbon steel in 3.5% NaCl solution using electrochemical, thermodynamic and theoretical studies using density functional theory (DFT).

2. Materials and methods

2.1 *Materials*

The weight percentage of API 5L Grade B carbon steel elements is shown in table 2. The experimental specimens were machined from steel pipe, soldered to copper wires and mounted with epoxy resin. The working electrode with a surface area of 0.785 cm^2 was abraded with waterproof abrasive papers. Isatin, 2-thiazoline-2-thiol, acetylcysteine and NaCl were provided by Merck Company. Blank solution was 3.5% NaCl prepared with distilled water. The inhibitor concentrations used were from 50 to 200 ppm.

2.2 *Synthesis*

A mixture of 2-thiazoline-2-thiol and isatin was used in refluxing absolute alcohol (100 ml) for 8 h at 70°C until 3, 4′-dihydro-3-[2′-mercaptothiazolidine]indol-2-one (DMI) was synthesized. After the completion of the reaction and 12 h crystallization at 0°C, orange crystals of DMI were formed and filtered.

The chemical synthesis of the inhibitor (DMI) and the structure of isatin and 2-thiazoline-2-thiol are shown in figure 1. The synthetization of DMI occurred by the condensation reaction of methylene and carbonyl groups of 2-thiazoline-2-thiol and isatin, respectively [20]. The chemical bonds of the synthesized organic corrosion inhibitor (DMI) were confirmed by Fourier transform infrared (FTIR) spectroscopy and nuclear magnetic resonance (NMR).

2.3 *Potentiodynamic polarization measurement*

Electrochemical measurements were obtained by using an Autolab Microautolab type III. In this work, the API 5L Grade B carbon steel samples were applied as working

Table 2. Chemical composition of carbon steel alloys in wt%.

Element	C	Si	Mn	P	S	Cr	Mo	Ni	Cu	V	Fe
Percentage (%)	0.11	0.28	0.76	0.01	0.002	0.07	0.009	0.1	0.08	0.05	Base

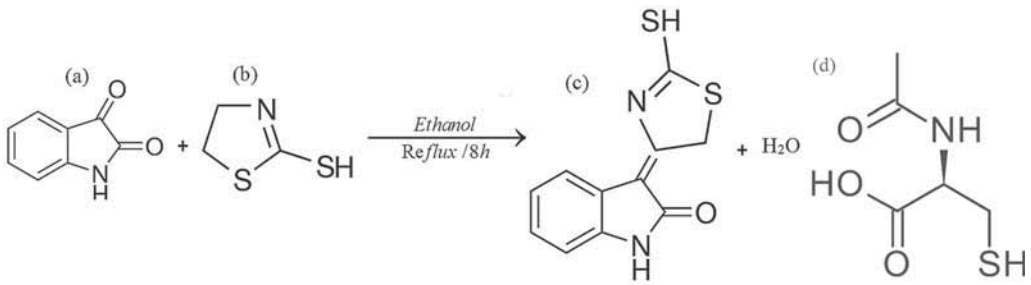

Figure 1. Chemical structures of (**a**) isatin, (**b**) 2-thiazoline-2-thiol, synthesized inhibitor, (**c**) DMI and (**d**) acetylcysteine.

electrodes. Furthermore, a silver–silver chloride (Ag/AgCl) as the reference and platinum as the counter electrode were used. The API 5L Grade B carbon steel specimens remained in the prepared solution for 60 min until the open circuit potential was reached. The scan rate of Tafel tests was 1.0 mV s^{-1} in an interval of −1000 to −400 mV. Calculations of potentiodynamic polarization parameters including anodic and cathodic Tafel slopes (β_a and β_c), potential of corrosion (E_{corr}), density of corrosion current (i_{corr}) and the inhibitor efficiency (IE%) were achieved using NOVA software. The inhibition efficiency was obtained from the below equation [21]:

$$IE\% = 100(1-I/I_0) \quad (2)$$

I and I_0 are the density of corrosion current in the presence and absence of the inhibitors, respectively, which were obtained from the polarization curves.

2.4 *Electrochemical impedance spectroscopy (EIS)*

EIS studies were employed using the 10 mV peak to peak in the frequency interval from 100 kHz to 10 mHz. ZSim software was used for the analysis of impedance data and the system temperature was controlled in a water bath.

2.5 *Surface characterization*

The scanning electron microscopy (SEM) images were obtained by using a QUANTA 200 instrument at a voltage of 20 kV and a magnification of 5k×. The specimen was immersed in 3.5% NaCl solution in blank and 200 ppm of the DMI solutions for 7 days. Then, the carbon steel samples were removed, washed and dried and then were observed by SEM.

2.6 *DFT calculations*

Quantum chemical calculations were carried out in the aqueous phase using the DFT method. B3LYP combined with 6–31G+(d,p) basis in the Gaussian 09W program was used. The important molecular parameters were calculated for the comparison of the inhibition performance of four inhibitors.

3. Results and discussion

3.1 *FTIR spectroscopy*

The structural characteristics of the synthesized product were confirmed by FTIR spectroscopy (Thermo AVATAR model) in the range of 4000–400 cm^{-1} (figure 2).

The characteristic band appeared for the out-of-plane bending C–H at 650 cm^{-1}, vibration of C–O at 1050 cm^{-1}, wagging mode of CH_2 at 1295 cm^{-1} [22] and the bending mode of N–H at 1515 cm^{-1}. The peak at about 1620 cm^{-1} was assigned to the bending vibrations of O–H water molecules, the bands at 1730 cm^{-1} were assigned to the stretching vibrations of the C=O band and the bands at 3140 and 3440 cm^{-1} were assigned to the vibrations of the N–H band [23].

NMR spectroscopy analysis of DMI was performed by using a Bruker Avance 400 MHz. Figures 3 and 4 show various ^1H and ^{13}C NMR spectra of DMI. Secondary amine (C–N–H) protons at the H15 position resonated at 9.60 ppm. The spectrum value appeared within 4.05 ppm was advocated in the presence of thiol (C–SH) in DMI (H23).

The ^{13}C NMR spectrum of DMI showed the signal of the amide group (O=C–N) at 176.45 ppm corresponding to C8. ^{13}C NMR spectra at 134.29 and 141.54 ppm corresponds to C16 and C2 positions indicated the presence of the (C–N) group in the DMI structure. Signals appeared at 130.54,

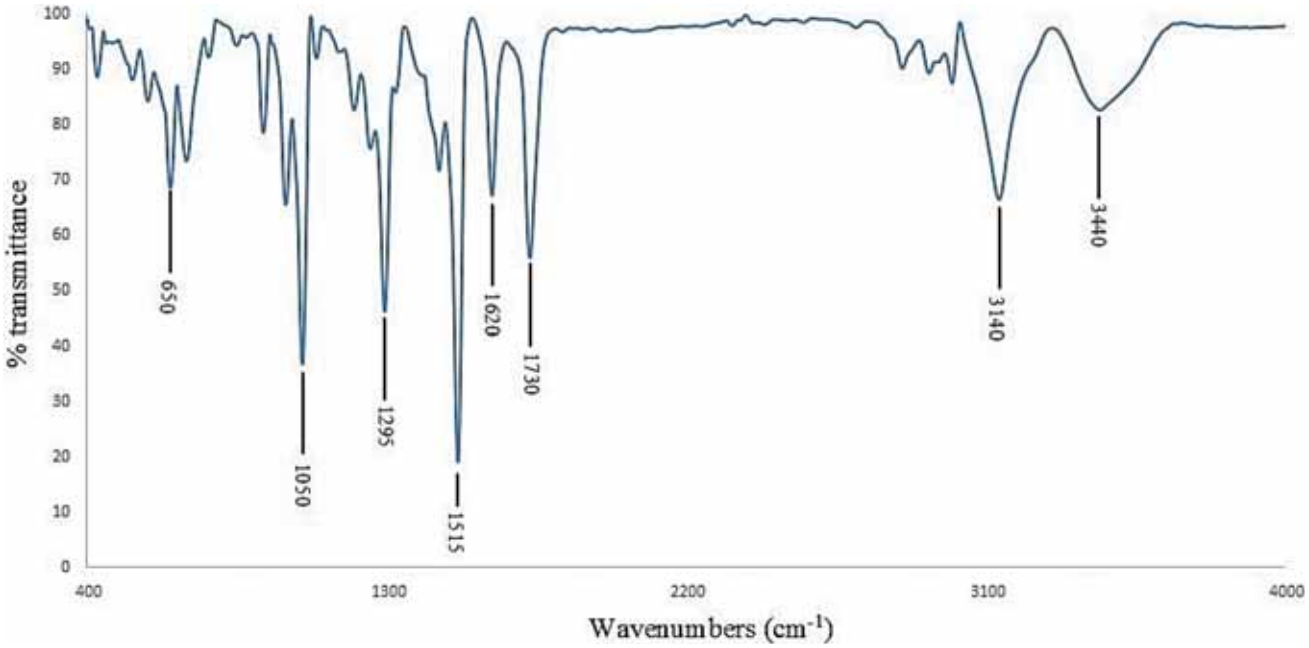

Figure 2. FTIR spectra of DMI.

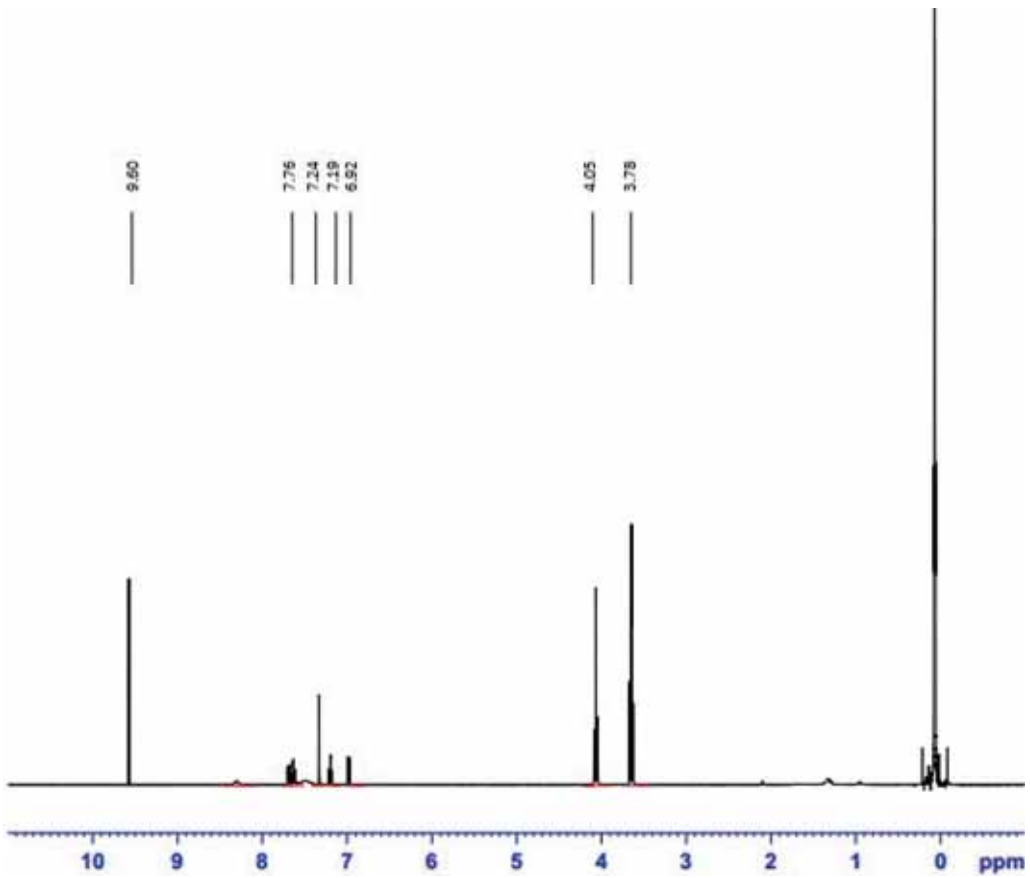

Figure 3. ^{1}H NMR spectra of DMI.

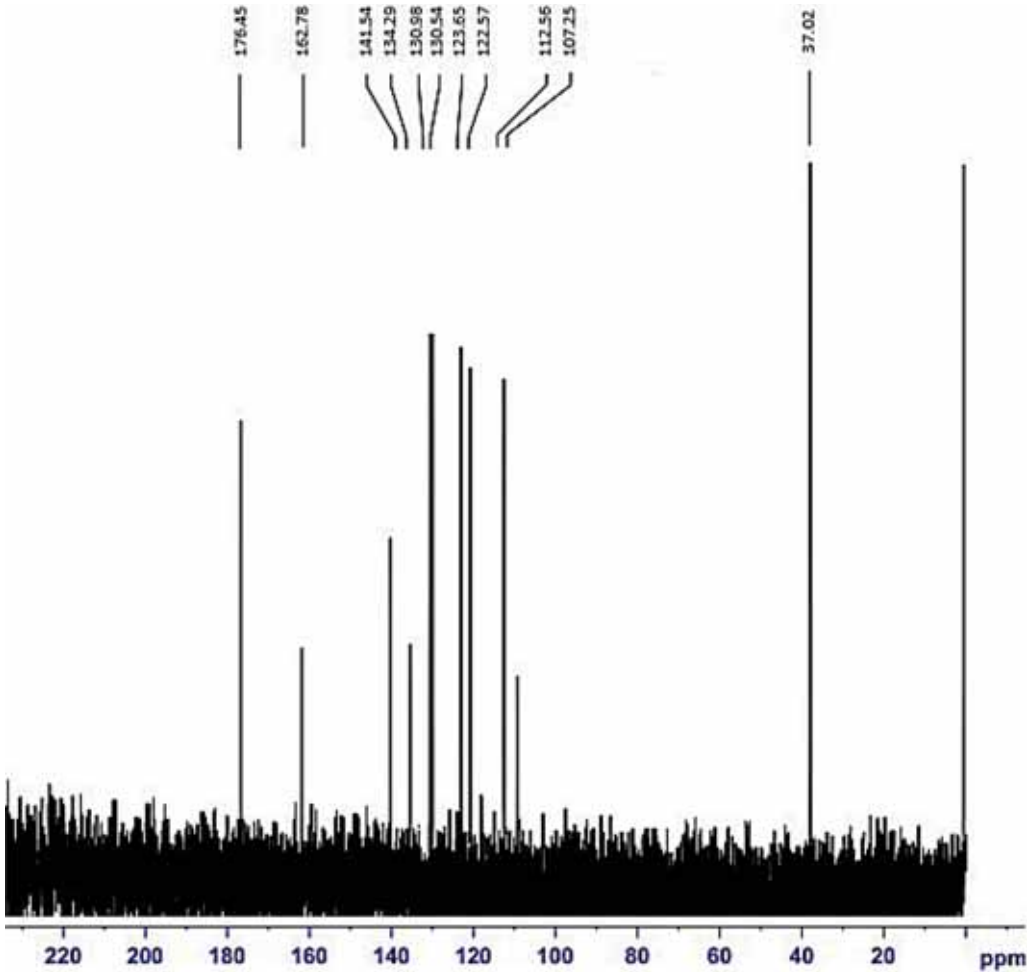

Figure 4. ^{13}C NMR spectra of DMI.

123.65 and 122.57 ppm were attributed to the presence of (C=C) in C4, C6 and C5 positions, respectively. The (C–C–N) showed the signal at 112.56 ppm, a signal at 107.25 ppm confirmed the presence of the (C–C–O) group and a signal at 37.02 ppm was attributed to carbon attached to the (S–CH_2) group in the DMI structure. All proton and carbon spectra were assigned and are shown in table 3, which matched with the molecular structure of DMI (figure 5) [24].

3.2 *Potentiodynamic polarization*

The potentiodynamic measurements in blank and the presence of DMI in solutions were studied by the curves of cathodic and anodic polarization as shown in figure 6. For more investigations three temperatures were tested (25, 45 and 65°C). The results were achieved in the 3.5% NaCl solution in various concentrations of DMI. As seen in figure 6, DMI was influenced on the cathodic and anodic polarization slopes. It means that DMI affected both the anodic dissolution of carbon steel electrodes and cathodic reduction in hydrogen evolution reactions, indicating that the type of the DMI corrosion inhibitor was mixed [25].

As the inhibitor concentration increased, a good inhibitor barrier layer was formed and corrosion current densities (i_{corr}) were decreased. The maximum inhibition efficiency (87%) was achieved at a concentration of 200 ppm DMI. With increasing inhibitor concentrations and temperatures, the E_{corr} values shifted to the cathodic regions. Also, the decrease of cathodic slopes was more than that of anodic ones. So, DMI decreased the cathodic corrosion reaction more than the anodic one [26].

Electrochemical corrosion parameters obtained by Tafel curves are listed in table 4. Changing the polarization slopes in the inhibited solution indicated that the inhibitor blocked the cathodic and anodic sites of the metal.

A comparison of the DMI corrosion inhibition performance with two reactants and acetylcysteine was performed. Tafel tests for 200 ppm of isatin, 2-thiazoline-2-thiol and acetylcysteine at 25°C were used (figure 6d). According to table 4, the efficiency of four inhibitors for 200 ppm at 25°C

Table 3. ^{1}H and ^{13}C NMR spectra of DMI.

^{1}H position	H20, 24	H23	H10	H12	H11	H13	H15
^{1}H NMR/ppm	3.78	4.05	6.92	7.19	7.24	7.76	9.60
^{13}C position	C17	C7	C3	C5	C6	C4	C1
^{13}C NMR/ppm	37.02	107.25	112.56	122.57	123.65	130.54	130.98
^{13}C position	C16	C2	C21	C8			
^{13}C NMR/ppm	134.29	141.54	162.78	176.45			

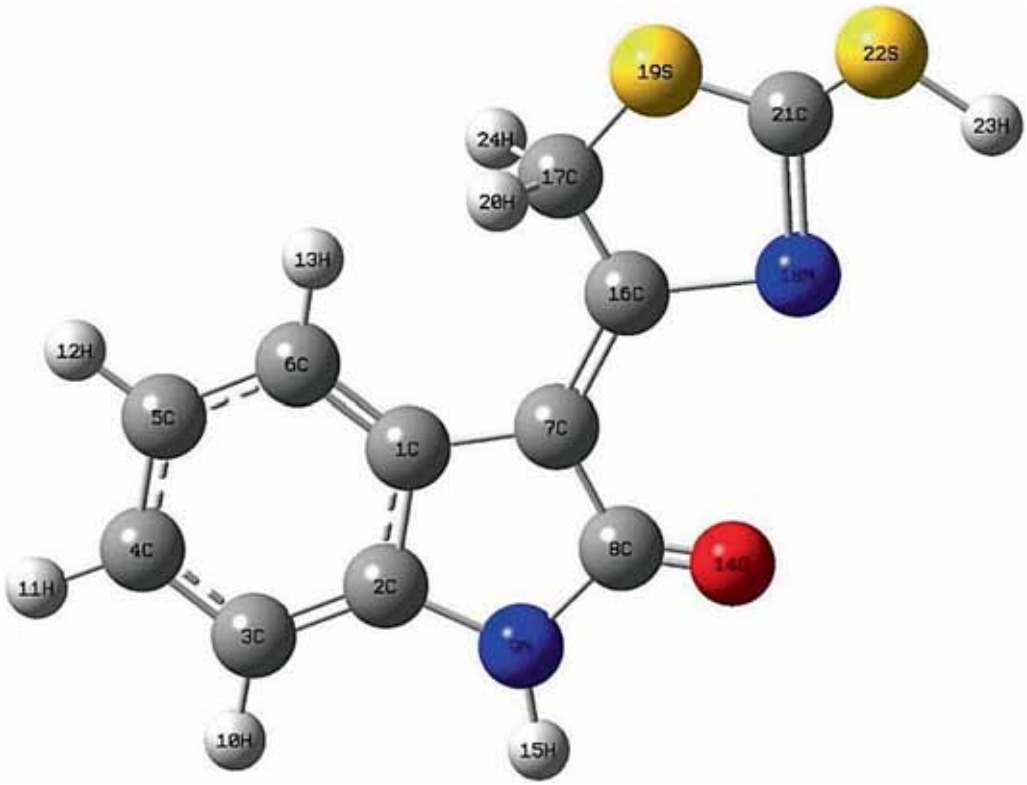

Figure 5. Numbering the atoms of DMI.

followed the following order: DMI (87%) > isatin (71%) > 2-thiazoline-2-thiol (62%) > acetylcysteine (54%).

Corrosion of carbon steel under a NaCl environment [27] obeyed the following reactions:

$$Fe \rightarrow Fe^{2+} + 2e^{-} \quad (3)$$

$$Fe^{2+} + 2Cl^{-} \rightarrow FeCl_2 \quad (4)$$

$$FeCl_2 + 2H_2O \rightarrow Fe(OH)_2 + 2H^{+} + 2Cl^{-} \quad (5)$$

$$Fe^{2+} \rightarrow Fe^{3+} + e^{-} \quad (6)$$

The reduction reaction is:

$$O_2 + 2H_2O + 4e^{-} \rightarrow 4OH^{-} \quad (7)$$

The corrosion reaction products ($Fe(OH)_2$) precipitated and yield complex compounds with oxygen, which include: FeOOH, FeO and Fe_2O_3. Cathodic Tafel branches in neutral solutions can be due to the formation of hydroxide reaction under diffusion control [28].

3.3 *EIS*

EIS studies were applied after 60 min immersion of API 5L Grade B carbon steel in the presence and absence of DMI in 3.5% NaCl solutions. Figure 7 demonstrates the plots of Nyquist in inhibited and uninhibited 3.5% NaCl solutions at 25°C with different concentrations of DMI. In order to investigate the electrochemical impedance with frequency an equivalent circuit was used which is shown in figure 7 [29].

In this circuit, R_s and R_{ct} are the solution resistance and the charge transfer resistance, respectively. Due to the charge transfer reaction, a constant phase element (CPE) in parallel to R_{ct} was required [30].

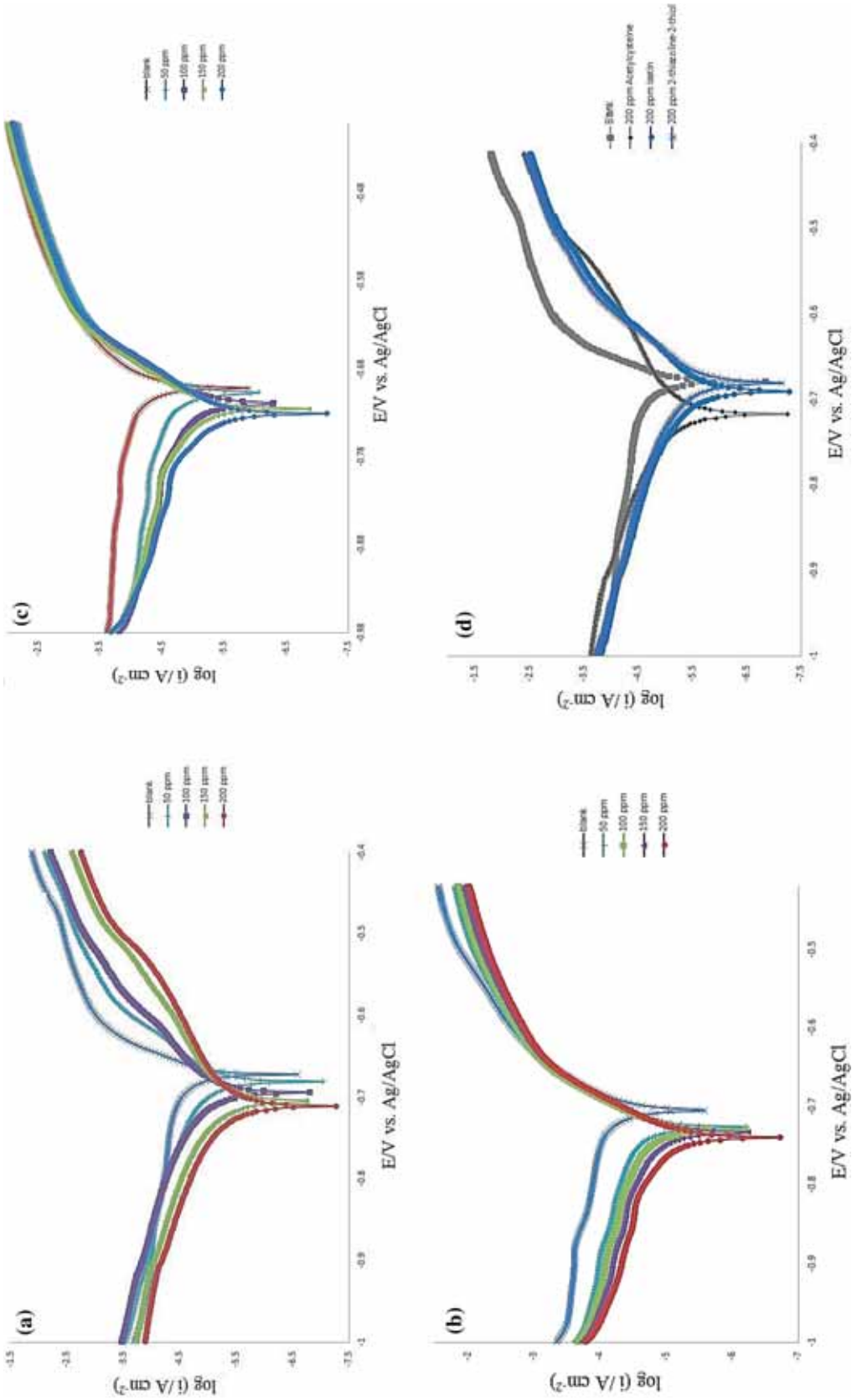

Figure 6. Anodic and cathodic polarization curves at (**a**) 25, (**b**) 45 and (**c**) 65°C without and with various concentrations of DMI. (**d**) Tafel curves with 200 ppm isatin, 2-thiazoline-2-thiol and acetylcysteine for carbon steel in 3.5% NaCl.

Table 4. Potentiodynamic polarization parameters obtained from the polarization curves of different DMI concentrations at different temperatures and 200 ppm concentrations of isatin, 2-thiazoline-2-thiol and acetylcysteine.

Inhibitor	Temp. (°C)	Conc. (ppm)	i_{corr} (μA cm^{-2})	E_{corr} (mV)	β_c (mV dec^{-1})	β_a (mV dec^{-1})	R_p (Ω cm^2)	C.R. (mm per year)	IE%	θ
DMI	25	Blank	51.10	−682.59	225.06	92.35	556.41	0.59	—	—
		50	23.9	−682.78	202.26	80.98	1050.61	0.27	53.22	0.53
		100	13.51	−682.91	165.82	68.56	1558.97	0.15	73.56	0.73
		150	8.88	−695.32	140.97	54.36	1918.36	0.10	82.62	0.82
		200	6.25	−707.53	135.24	50.54	2556.03	0.07	87.76	0.87
Isatin	25	200	14.14	−683.8	215.93	71.63	2936.20	0.16	71.82	0.71
2-Thiazoline-2-thiol	25	200	19.48	−673.70	220.06	86.83	2225.30	0.22	62.02	0.62
Acetylcysteine	25	200	23.14	−725.65	223.25	93.45	860.82	0.32	54.71	0.54
DMI	45	Blank	85.09	−711.86	295.65	74.80	304.6333	0.98	—	—
		50	36.36	−723.42	280.91	68.24	655.6565	0.42	57.26	0.57
		100	20.78	−731.27	256.16	60.98	1029.22	0.24	75.57	0.75
		150	12.12	−727.90	224.76	54.58	1573.341	0.14	85.75	0.85
		200	9.23	−736.80	203.65	50.13	1892.47	0.10	89.15	0.89
DMI	65	Blank	106.35	−709.66	296.10	111.57	330.86	1.23	—	—
		50	33.34	−713.98	245.55	93.17	879.66	0.38	68.65	0.68
		100	18.74	−728.58	215.45	84.3	1403.94	0.21	82.37	0.82
		150	9.93	−731.14	205.25	77.11	2451.02	0.11	90.66	0.90
		200	7.02	−737.78	195.92	64.95	3017.19	0.08	93.39	0.93

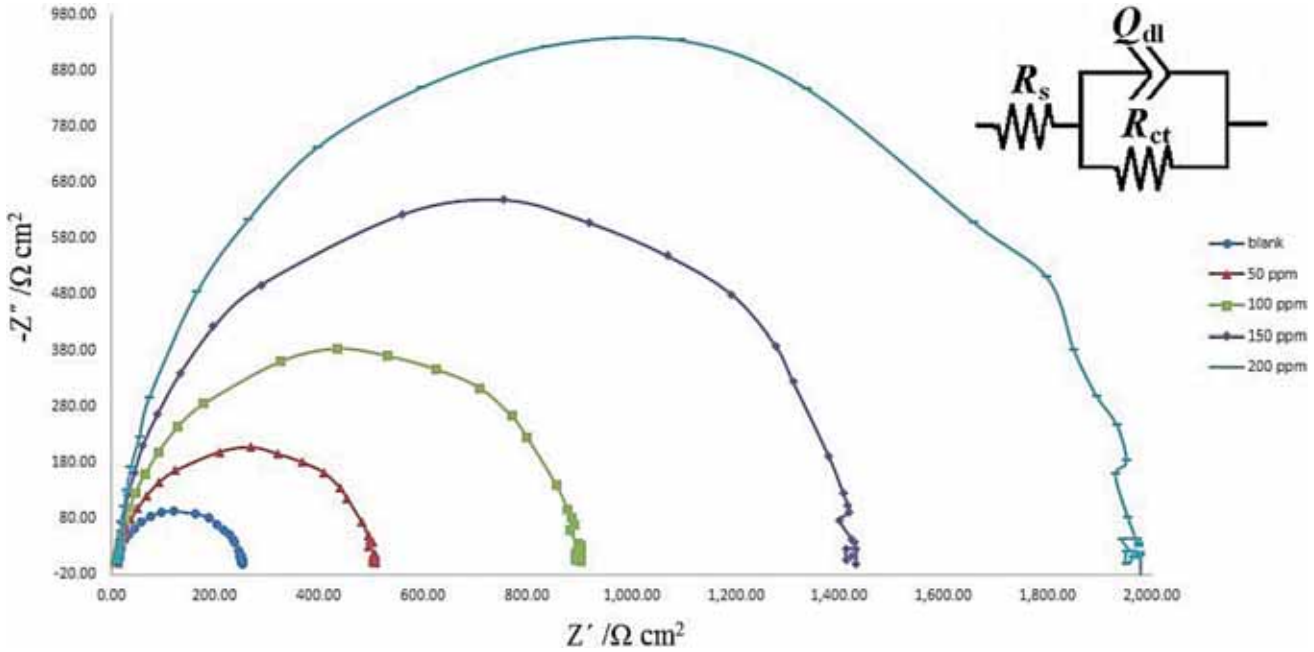

Figure 7. Nyquist plots and equivalent circuit for steel in 1 M HCl containing different concentrations of DMI at 25°C.

Figure 7 illustrates that as the inhibitor concentration increased the charge transfer resistance (R_{ct}) increased. Single semicircles in these plots showed the single time constant and indicated the corrosion reaction controlled by the charge transfer process. The cause of deviation in semicircles of the plots was due to the inhomogeneity of the steel surface [31].

By adding DMI into the solution, the shape of the semicircles remained fixed indicating that no change in the mechanism of the adsorbed inhibitor film occurred. The value of the CPE impedance is determined by following relationship [32]:

$$Z_{CPE} = 1/Q(i\omega)^n. \tag{8}$$

In this formula Q is a parameter of capacitive and n is related to the constant phase angle. Nyquist plots were fitted with an equivalent circuit using ZSim software and EIS parameters such as double layer capacitance (C_{dl}), R_{ct}, R_s, Q, n and τ were calculated and are shown in table 5.

According to table 5, the Q values were lower in the presence of DMI with respect to the uninhibited solution. It indicates the substitution of the inhibitor for H_2O molecules and the formation of the barrier layer. The double layer capacitance (C_{dl}) values decreased in the presence of DMI due to the increase in the thickness of the electrical double layer protective film. This behaviour is described by the Helmholtz equation [33]:

$$C_{dl} = \varepsilon\varepsilon_0 S/e. \tag{9}$$

In this equation ε is the medium dielectric constant, ε_0 is the vacuum permittivity, S is the exposed surface area and e is the thickness of the protective film.

The value of n for 3.5% NaCl medium was low indicating that the inhomogeneity of the surface was a result from corrosion. With the addition of DMI concentrations the n value increased from 0.85 to 0.97 indicating that the increase in surface homogeneity was because of the inhibitor adsorption film. Moreover, as DMI concentration increased the value of the relaxation time constant ($\tau = RC$) increased and illustrated the slow adsorption process [34].

3.4 *Adsorption isotherm and thermodynamic parameters*

Adsorption isotherms provided information of adsorption mechanisms such as the adsorption equilibrium constant, coverage of surface and metal surface and inhibitor molecule interactions [35]. Adsorption isotherms were used for studying the corrosion inhibitors and metal surface interactions more accurately.

In this work three important isotherms (Langmuir, Frumkin and Temkin) were used to fit according to below equations [36]:

$$\text{Langmuir: } \theta/1-\theta = K_{ads}C, \tag{10}$$

$$\text{Temkin: } \log\theta/C = \log K - g\theta, \tag{11}$$

$$\text{Frumkin: } \log\theta/(1-\theta)C = \log K_{ads} + g\theta. \tag{12}$$

The correlation coefficients (R^2) of isotherm diagrams were evaluated to select the best fit one.

Table 5. Impedance data for steel in 3.5% NaCl solution without and with different concentrations of DMI at 25°C.

DMI Conc. (ppm)	R_s (Ω cm^2)	R_{ct} (Ω cm^2)	$C_{dl} \times 10^5$ (F)	Q_{dl} or Y_O ($s^n\,\Omega^{-1}cm^{-2}$)	n	τ (s)
Blank	7.45	190.67	10.1327	0.000225	0.85	0.024
50	8.90	389.12	9.22518	0.000165	0.89	0.045
10	8.28	697.94	5.83426	0.000097	0.91	0.051
150	10.51	1097.43	3.33059	0.000051	0.94	0.04
200	11.53	1528.39	0.90402	0.000013	0.97	0.017

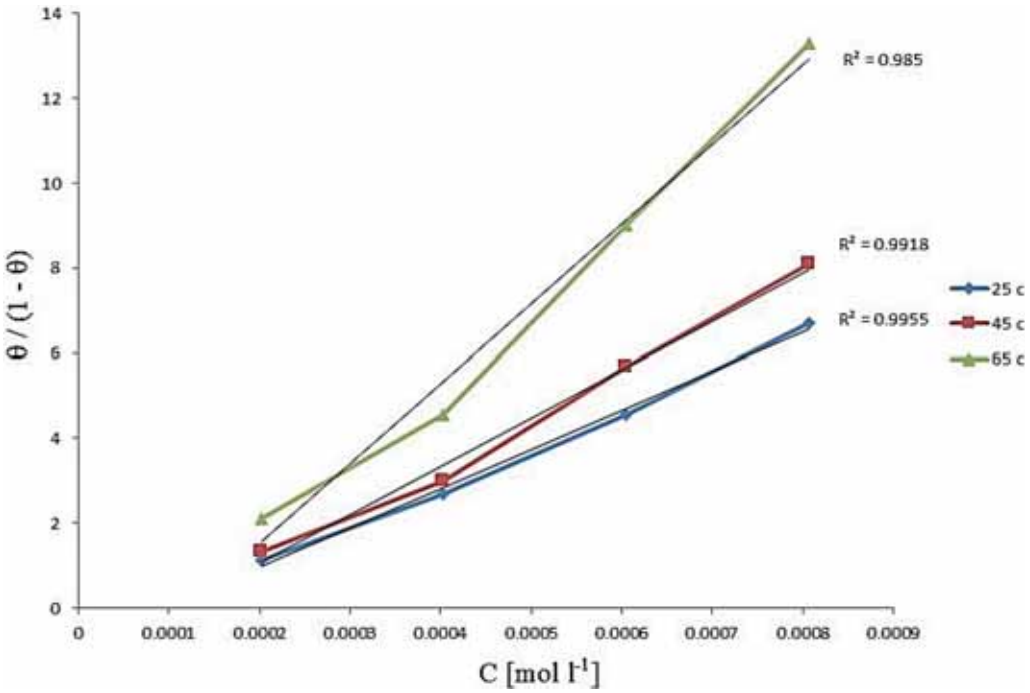

Figure 8. Langmuir adsorption plots of steel in 3.5% NaCl and containing various concentrations of DMI at 25, 45 and 65°C.

The best fit of DMI experimental data in 3.5% NaCl solution was observed in Langmuir adsorption isotherms with $R^2 = 0.98$ which describes that the adsorption inhibitors have no interaction with the steel surface [37]. The plots of $\theta/1-\theta$ *vs. C* in different concentrations of inhibitors and three temperatures are shown in figure 8.

The values of K_{ads} at different temperatures were calculated using Langmuir adsorption equations (table 6). The high values of K_{ads} implicated a strong chemisorption adsorption bond. Activation parameters including standard entropy (ΔS°) and standard enthalpy (ΔH°) can be achieved by this equation:

$$I_{corr} = (RT/Nh)\exp(-\Delta H^\circ/RT)\exp(\Delta S^\circ/R). \quad (13)$$

In this equation N is the Avogadro's number and h is the Planck constant. $\mathrm{Log}(I_{corr}/T)$ against $1/2.303RT$ (figure 9) lines were used for computed activation thermodynamic parameters (ΔH° and ΔS°) as shown in table 7.

The slopes and intercepts of these lines were $(-\Delta H^\circ)$ and $(\log R/Nh + \Delta S^\circ/2.303R)$, respectively [38]. The negative sign of activation entropy (ΔS°) values indicated the reduction in disorder [39].

K_{ads} values could be used for the calculation of ΔG°_{ads} values according to the Gibbs–Helmholtz equation as follows:

$$\Delta G^\circ_{ads} = -RT\ln(55.5K_{ads}). \quad (14)$$

From table 6, the large negative values of ΔG°_{ads} verified the spontaneous phenomenon and the stability of the adsorption film formation. The value of ΔG°_{ads} up to -20 kJ mol^{-1} illustrated the physisorption according to Van der Waals forces between the inhibitor and the surface of the metal, while the values more negative than

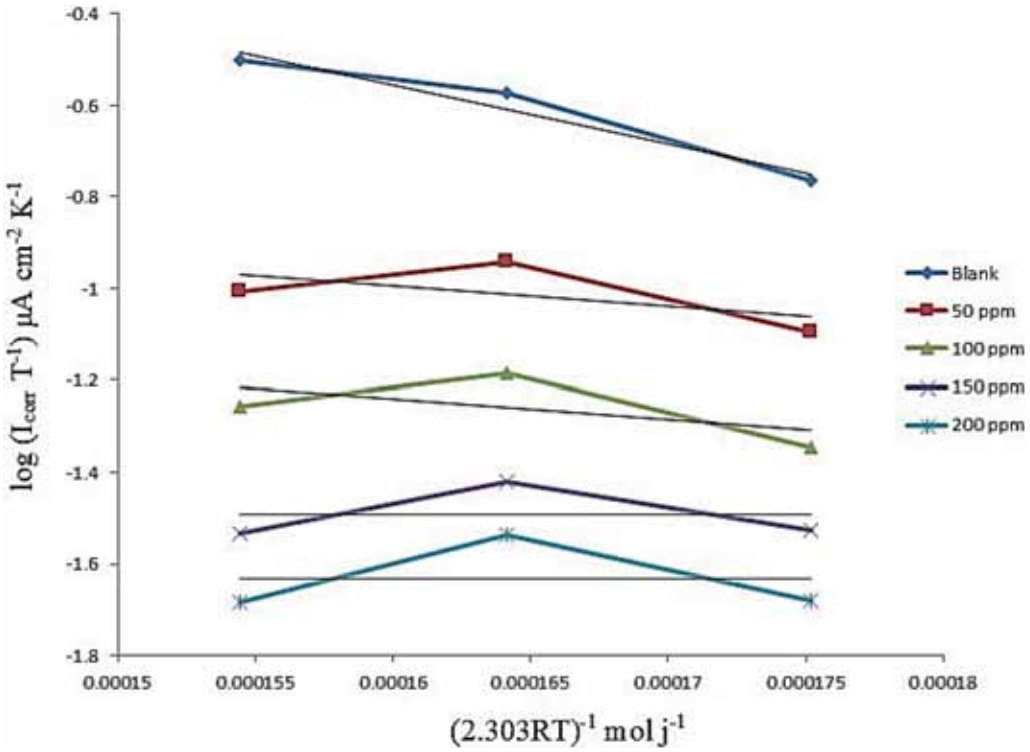

Figure 9. Transition state plots for steel corrosion in 3.5% NaCl in the absence and presence of different concentrations of DMI.

Table 6. Adsorption equilibrium constants and standard free energies of adsorption.

Temperature (°C)	K_{ads} (M^{-1})	ΔG°_{ads} (kJ mol^{-1})
25	9198.7	−32.58
45	11,389	−35.33
65	18,812	−38.96

Table 7. Activation parameters of steel in 3.5% NaCl solution in the presence of DMI.

DMI conc. (ppm)	$\Delta H_{act.}$ (kJ mol^{-1})	$\Delta S_{act.}$ (kJ mol^{-1})	$\Delta G_{act.}$ (kJ $mol^{-1}K^{-1}$) Temperature (K)		
			298.15	318.15	338.15
Blank	245.67	−0.16	296.03	299.40	302.78
50	87.17	−0.20	147.59	151.65	155.70
100	85.14	−0.20	147.07	151.22	155.38
150	1.41	−0.22	68.90	73.43	77.96
200	1.64	−0.22	69.79	74.36	78.93

−40 kJ mol^{-1} shows chemisorption [40]. The ΔG°_{ads} values obtained in this study were around −40 kJ mol^{-1} revealing that the DMI adsorption on steel was mostly chemisorption [41].

The Van't Hoff equation could be used for more thermodynamic studies of DMI adsorption. Enthalpy (ΔH°_{ads}) and entropy of adsorption (ΔS°_{ads}) were calculated from this equation [42]:

$$\ln K_{ads} = -\Delta H^{\circ}_{ads}/RT + \Delta S^{\circ}_{ads}/R + \ln(1/55.5). \quad (15)$$

A graph of $\ln K_{ads}$ *vs.* $1/T$ straight lines with the $\Delta S^{\circ}_{ads}/R + \ln(1/55.5)$ intercept and the $-\Delta H^{\circ}_{ads}/R$ slope was used for calculating the adsorption parameters. The Gibbs–Helmholtz formula is another way to calculate the adsorption enthalpy as follows:

$$\Delta G^{\circ}_{ads}/T = \Delta H^{\circ}_{ads}/T + K. \quad (16)$$

Furthermore, heat of adsorption (ΔH°_{ads}) and adsorption entropy (ΔS°_{ads}) could be found according to the common equation of thermodynamics [43]:

$$\Delta G^{\circ}_{ads} = \Delta H^{\circ}_{ads} - T\Delta S^{\circ}_{ads} \quad (17)$$

$-\Delta S^{\circ}_{ads}$ is the slope of ΔG°_{ads} *vs.* T straight line and ΔH°_{ads} is the intercept of this plot. For this inhibitor, ΔH°_{ads} and ΔS°_{ads}

Table 8. Thermodynamic and equilibrium adsorption parameters.

Different thermodynamic equations	ΔH_{ads} (kJ mol^{-1})	ΔS_{ads} (kJ mol^{-1} K^{-1})
Basic thermodynamic equation	15.14	0.15
Van't Hoff equation	14.84	0.15
Gibbs–Helmholtz equation	14.84	—

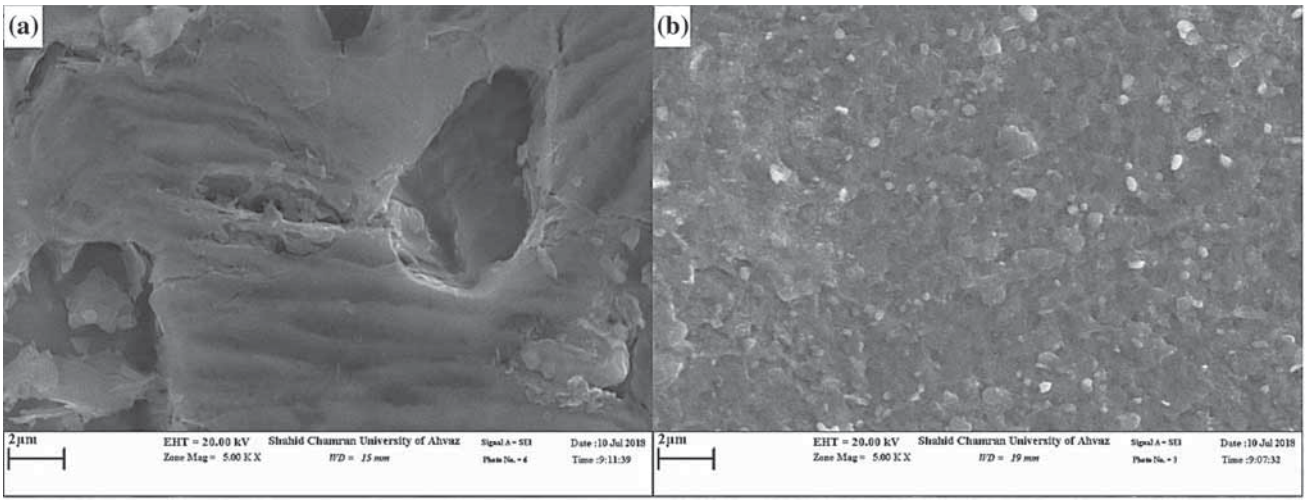

Figure 10. SEM surface topography images immersed for 7 days in 3.5% NaCl: (**a**) uninhibited and (**b**) inhibited solution with 200 ppm DMI at 25°C.

values are shown in table 8. The values of ΔH°_{ads} and ΔS°_{ads} obtained from the three thermodynamic equations were in good agreement.

The positive sign of ΔH°_{ads} inferred the endothermic adsorption process and had been attributed to chemical adsorption. The value of ΔH°_{ads} gained in this work (14.84 kJ mol^{-1}) suggests the chemisorption mode for DMI [44].

DMI is a heterocyclic compound and is adsorbed on the surface of carbon steel. The adsorption on anodic sites occurred through long π-electrons of aromatic rings and lone pairs of electrons of nitrogen, sulphur and oxygen atoms, which decreased the anodic dissolution of mild steel. The functional groups of DMI molecules were more efficient than those in isatin, 2-thiazoline-2-thiol and acetylcysteine. Ketone C=O and secondary amine R1R2-NH functional groups in isatin and thiol S–H and sulphide and nitrogen in 2-thiazoline-2-thiol structures were combined for synthetization of DMI. So, DMI had more and stronger heteroatoms for donating electrons. Coordinate covalent bonds were formed by donor–acceptor interactions between electron pairs of unprotonated N, O and S atoms in ketone, mercaptothiazoline and indole ring functional groups of DMI with the vacant and low energy d-orbitals of iron [45]. In the cationic form with the positively charged part of the molecule oriented toward the negatively charged carbon steel surface, the protonated species of the inhibitor adsorb on the cathodic sites of the mild steel and retard the evolution of hydrogen. Furthermore, the long hydrocarbon chain length in the molecular structure of DMI when compared to that of other inhibitors attributed to the increase in the adsorption ability of the compound on the metal surface because of the increase in the molecular size [46].

3.5 *Surface study*

SEM is a helpful and practical surface method to observe the morphological features of metal and alloy surfaces [47]. As shown in figure 10a, the steel surface in uninhibited solution is highly damaged because of the high iron dissolution rate in corrosive media and attack of 3.5% NaCl solution. However, the SEM image of the inhibited steel surface appeared to be smooth (figure 10b). The smooth area of the steel surface with DMI molecules has shown excellent inhibition of the surface due to the protective and barrier film.

3.6 *DFT calculations*

Quantum chemical calculations of reactants, DMI and acetylcysteine have been performed by the DFT/B3LYP complemented with the basis set 6–31G+(d,p).

The inhibitory effect of corrosion inhibitor molecular functional group and the structure of the synthesis corrosion

Table 9. Quantum chemical parameters derived from the B3LYP/6–31+G(d,p) method.

Inhibitors	E_{HOMO} (eV)	E_{LUMO} (eV)	ΔE (eV)	η (eV)	S (eV^{-1})	ΔN	μ (D)
DMI	−5.88	−2.47	3.40	1.70	0.29	0.82	4.83
2-Thiazoline-2-thiol	−6.67	−0.78	5.88	2.94	0.17	0.55	3.23
Isatin	−6.55	−2.65	3.89	1.95	0.25	0.61	5.93
Acetylcysteine	−6.91	−0.90	6.01	3.00	0.16	0.51	5.46

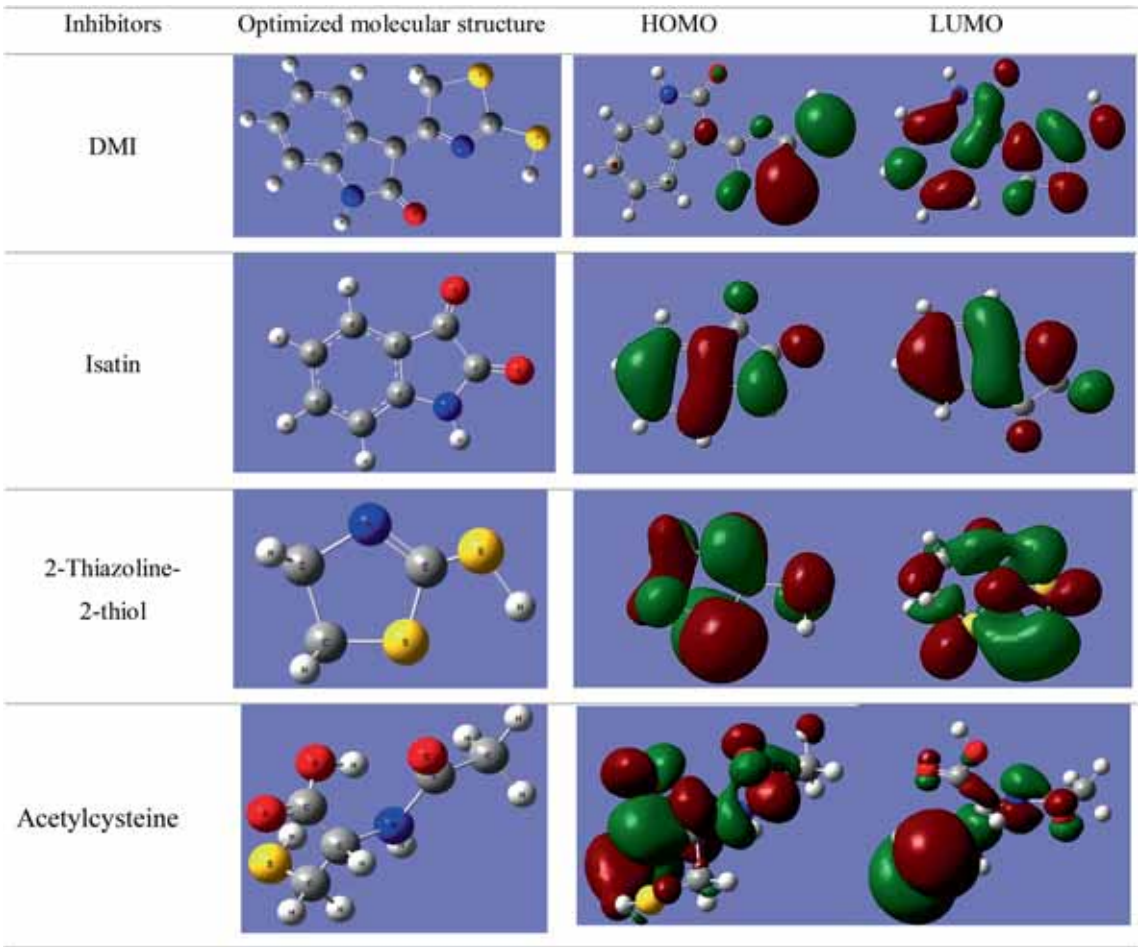

Figure 11. Optimized molecular structures, HOMO and LUMO electron density isosurfaces of four inhibitors obtained at the B3LYP/6–31G + (d,p) level of theory.

inhibitor (DMI), reactants (isatin and 2-thiazoline-2-thiol) and acetylcysteine were discussed by a quantum chemistry study. To explain the potentiodynamic experimental results and to achieve a dominant mechanism for the inhibition of DMI against corrosion, quantum chemical calculations were used.

The important molecular parameters such as the energy of the lowest unoccupied molecular orbital (E_{LUMO}), energy of the highest occupied molecular orbital (E_{HOMO}), difference between E_{LUMO} and E_{HOMO} which is the energy gap (ΔE), chemical hardness (η), dipole moment (μ), softness (S) and the fraction of electrons transferred (ΔN) were calculated and are listed in table 9 [48]. The equations of these parameters are shown as below [49]:

$$\eta = (1/2)(\partial N/\partial \mu)_{\upsilon(r)} = (\partial^2 E/\partial N^2)_{\upsilon(r)}, \quad (18)$$

$$S = 1/2\eta = (\partial N/\partial \mu)_{\upsilon(r)}, \quad (19)$$

$$\Delta N = (\chi_M - \chi_{inh})/[2(\eta_M + \eta_{inh})], \quad (20)$$

where χ is electronegativity and N is the electron number [50]. The E_{HOMO} value shows the ability of the inhibitor compound to give electrons to a receiver one, while the E_{LUMO} indicates the ability of the compound to

receive electrons. High E_{HOMO} values illustrated the high tendency of a molecule to give electrons and a low value of the E_{LUMO} demonstrated that the molecule received electrons easily. The energy gap (ΔE) shows the tendency of species to transfer electrons to the metal. When ΔE increases, the inhibitor efficiency decreases due to the decrease in adsorption [51].

The E_{HOMO}, E_{LUMO} and ΔE values in table 9 show that, in comparison with isatin, 2-thiazoline-2-thiol and acetylcysteine, DMI had the smallest value of energy gap (3.40 eV) and the highest corrosion inhibition performance.

The dipole moment (μ) is an important parameter for the evaluation of inhibitor molecules. The high value of dipole moment is a sign of good corrosion inhibition of a molecule. In this study, the dipole moment value of DMI was the biggest value (4.83 eV) and showed excellent inhibition action [52].

Absolute softness (S) and hardness (η) are important parameters to evaluate the ability of the molecular reaction. Hard molecules are less reactive and more stable than soft ones [53]. In this work DMI has the highest softness ($0.29\ eV^{-1}$) and the lowest hardness (1.70 eV) values, therefore it has the best inhibition performance. The inhibitor molecule fraction of electrons (ΔN) that moved to the metal surface was determined by equation (20).

Increasing the fraction of electrons (ΔN) leads to an increase in the inhibition efficiency and stronger adsorption [54]. Lukovits illustrated that if $\Delta N < 3.6$, the corrosion inhibitor molecule tends to give the electron and the corrosion inhibitor efficiency increased as the electrophilicity of the molecule increased [55]. The number of electrons transferred (ΔN) from four corrosion inhibitors are shown in table 9. It is clear that the ΔN values in all four inhibitors are less than 3.6 and this value for DMI is greatest that illustrated the high tendency of DMI molecule adsorption in comparison with other inhibitors.

In figure 11, HOMO, LUMO electron density isosurfaces and optimized molecular structures of four inhibitors are shown. The red (negative) regions of the HOMO and LUMO orbitals were demonstrated to be nucleophilic and the blue (positive) areas are related to electrophilic reactivity. These figures show that the nucleophilic regions of the inhibitor molecules are mainly localized near the conjugated double bonds and heteroatoms, which easily shared electrons with metallic atoms and formed chemisorption [56].

For estimation of local interactions of donor and acceptor electrons and the charge distribution over the molecule structure, the electrophilic Fukui function during loss of electrons data was utilized to investigate the reaction ability of each atom in the DMI molecule as follows [57]:

$$f_K^- = q_K(N) - q_K(N-1) \tag{21}$$

q_K is the charge of the atom (K), N denotes the electron number and N–1 is applied for the cation of the molecule [58].

Table 10. Calculated atomic charge distribution and Fukui indices for DMI.

Atom no.	Atom	q_N	q_{N-1}	f_K^-
14	O	−0.631	−0.403	−0.228
17	N	−0.07	0.035	−0.105
20	S	0.156	0.324	−0.168
22	S	0.154	0.320	−0.166

As heteroatoms are more negatively charged, the more ability of molecules to absorb on the metal surface was observed [59]. Numbering the atoms of DMI is shown in figure 5.

From table 10 it can be observed that the atoms of O (14) in the indole group, N (17), S (20) and S (22) in thiazole and thiol groups are the most negative and active regions, respectively. These results showed the essential effect of heteroatoms in corrosion inhibitor adsorption.

4. Conclusions

The synthesized DMI performed as a good corrosion inhibitor for carbon steel in 3.5% NaCl and showed 87% inhibition efficiency in 200 ppm at 25°C. This compound was characterized by FTIR.

The polarization curves showed an increasing efficiency with an increase in the concentration of DMI and temperature and indicated that the inhibitor molecules inhibit both anodic and cathodic reactions and are classified as mixed type inhibitors. EIS studies showed the increase in the charge transfer resistance of carbon steel at interfaces of metal and solution. The Langmuir adsorption isotherm model of DMI was adopted.

It could be concluded that the magnitude of ΔG°_{ads}, the sign of ΔH°_{ads} and a decrease in double layer capacitances are evidence that the adsorption of DMI occurred through chemisorption. The SEM images revealed an excellent protective film present on the surface. The theoretical DFT parameters and experimental results obtained for DMI, reactants and acetylcysteine confirmed each other as well.

References

[1] Shetty S and Shetty P 2007 *Mater. Lett.* **61** 2347
[2] Ivušić F, Lahodny-Šarc O and Alar V 2013 *Materialwiss. Werkst.* **44** 319
[3] Sastri V 1998 *Corrosion inhibitors: principles and applications* (New York: Wiley)
[4] Noor E A and Al-Moubaraki A H 2008 *Mater. Chem. Phys.* **110** 145
[5] Kadhim A, Al-Okbi A K, Jamil D M, Qussay A, Al-Amiery A A, Gaaz T S *et al* 2017 *Results Phys.* **7** 4013

[6] Niu L, Zhang H, Wei F H, Wu S X, Cao X L and Liu P P 2005 *Appl. Surf. Sci.* **252** 1634
[7] Khan G, Basirun W J, Kazi S N, Ahmed P, Magaji L, Ahmed S M *et al* 2017 *J. Coll. Interface Sci.* **502** 134
[8] Qiang Y, Zhang S, Yan S, Zou X and Chen S 2017 *Corros. Sci.* **126** 295
[9] Zheludkevich M L, Yasakau K A, Poznyak S K and Ferreira M G S 2005 *Corros. Sci.* **47** 3368
[10] Oguzie E E, Adindu C B, Enenebeaku C K, Ogukwe C E, Chidiebere M A and Oguzie K L 2012 *J. Phys. Chem. C* **116** 13603
[11] Ahmed Ali M A 2016 Thesis for the degree of Master of Engineering, University of Manchester School of Materials
[12] Lata S and Chaudhary R 2008 *Indian J. Chem. Technol.* **12** 364
[13] Ibrahim I, Kassim E S M, Jai J, Daud M and Hashim M A 2018 *Int. J. Eng. Technol.* **7** 316
[14] Velranil S, Jeyaprabha B and Prakash P 2014 *Int. J. Innov. Sci. Eng. Technol.* **1** 57
[15] Kassim E S M, Jai J, So'aib M S, Zamanhuri N A, Husin H and Hashim M A 2018 *Mater. Sci. Eng.* **358** 12045
[16] Ivušić F, Lahodny-Šarc O and Stojanović I 2014 *Tehnicki Vjesnik* **21** 107
[17] Rivera-Graul M, Casales M, Regla I, Ortega-Toledo D M, Ascencio-Gutierrez J A, Porcayo-Calderon J *et al* 2013 *Int. J. Electrochem. Sci.* **8** 2491
[18] Kassoul O, Galai M, Ballakhmima R A, Dkhireche N, Rochdi A, Ebn Touhami M *et al* 2015 *J. Mater. Environ. Sci.* **6** 1147
[19] Nwanebu C E 2015 MSc Thesis, Department of Chemical Engineering, McGill University, Montreal
[20] Pardasani R T, Pardasani P, Muktawat S and Chaturvedi V 1998 *Sulfur Silicon* **142** 221
[21] Rocchini G 1992 *Corros. Sci.* **11** 1759
[22] Singlit Y and Li S 1994 *Specnochim. Acta* **3** 509
[23] Sondhi S, Rani R, Gupta P, Agrawal S and Saxena A 2009 *Mol. Divers.* **13** 357
[24] Pretsch E, Buhlmann P and Badertscher M 2009 *Structure determination of organic compounds* (Berlin Heidelberg: Springer-Verlag)
[25] Hassan H H, Abdelghani E and Amin M A 2007 *Electrochim. Acta* **52** 6359
[26] Ansari K R, Quraishi M A and Ebenso E 2013 *Int. J. Electrochem. Sci.* **8** 12860
[27] Saker S, Aliouane N, Hammache H, Chafaa S and Bouet G 2015 *Ionics (Kiel)* **21** 2079
[28] Zhao J, Duan H and Jiang R 2015 *Corros. Sci.* **91** 108
[29] Zhou C, Lu X, Xin Z, Liu J and Zhang Y 2014 *Corros. Sci.* **80** 269
[30] Wu X J, Ma H Y and Chen S H 1999 *J. Electrochem. Soc.* **146** 1847
[31] Lebrini M, Lagrenée M, Traisnel M, Gengembre L, Vezin H and Bentiss F 2007 *Appl. Surf. Sci.* **253** 9267
[32] Macdonald J R 1987 *J. Electroanal. Chem. Inter. Electrochem.* **223** 25
[33] Hsu C H and Mansfeld F 2001 *Corros.* **57** 747
[34] Growcock F B and Jasinski R J 1989 *J. Electrochem. Soc.* **136** 2310
[35] Zhang G, Chen C, Lu M, Chai C and Wu Y 2007 *Mater. Chem. Phys.* **105** 331
[36] Faustin M, Maciuk A, Salvin P, Roos C and Lebrini M 2015 *Corros. Sci.* **92** 287
[37] Elayyachy M, El Idrissi A and Hammouti B 2006 *Corros. Sci.* **48** 2470
[38] Ramesh S V and Adhikari V 2007 *Bull. Mater. Sci.* **31** 699
[39] Abd El-Rehim S S, Hassan H H and Amin M A 2001 *Mater. Chem. Phys.* **70** 64
[40] Duan S Z and Tao Y L 1990 *Interface chemistry* Vol 124 (Beijing: Higher Education Press)
[41] Branzoi V, Baibarac M and Branzoi F 2001 *Sci. Bull. B Chem. Mater. Sci.* **63** 9
[42] Han P, Chen C, Li W, Yu H, Xu Y, Ma L *et al* 2018 *J. Colloid Interface Sci.* **516** 398
[43] Morad S and Kamal El-Dean A M 2006 *Corros. Sci.* **48** 3398
[44] Zarrouk H, Salghi R, Assouag M, Hammouti B, Oudda H, Boukhris S *et al* 2013 *Der. Pharm. Lett.* **5** 43
[45] Samide A, Bibicu I, Rogalski M and Preda M 2004 *Acta Chim. Slov.* **51** 127
[46] Abdel-Gaber A M, Abd-El-Nabey B A and Saadawy M 2009 *Corros. Sci.* **51** 1038
[47] Li W, He Q, Pei C and Hou B 2007 *Electrochim. Acta* **52** 6386
[48] Kabanda M M, Murulana L C, Ozcan M, Karadag F, Dehri I, Obot I B *et al* 2012 *Int. J. Electrochem. Sci.* **7** 5035
[49] Sastri V S and Perumareddi J R 1997 *Corros. Sci.* **53** 617
[50] Gece G and Bilgic S 2010 *Corros. Sci.* **52** 3435
[51] Awad M K 2004 *J. Electroanal. Chem.* **567** 219
[52] Ebenso E, Isabirye D and Eddy N 2010 *Int. J. Molecul. Sci.* **11** 2473
[53] Gece G and Bilgic S 2009 *Corros. Sci.* **51** 1876
[54] Hamid S M and Sherrington D C 1984 *J. Brit. Polym.* **16** 245
[55] ElBelghitia M, Karzazi Y, Dafali A, Hammouti B, Bentiss F, Obot I B *et al* 2016 *J. Mol. Liq.* **218** 281
[56] Kikuchi O 1987 *Quant. Struct. Act. Relat.* **6** 179
[57] Scendo M 2007 *Corros. Sci.* **49** 373
[58] Li W, Zhao X, Liu F and Hou B 2008 *Corros. Sci.* **50** 3261
[59] Daoud D, Douadi T, Hamani H, Al-Noaimi M and Chafaa S 2015 *Corros. Sci.* **94** 21